

1 **Last ice sheet recession and landscape emergence above sea level in east-central Sweden, evaluated**  
2 **using *in situ* cosmogenic  $^{14}\text{C}$  from quartz**

3

4 Bradley W. Goodfellow<sup>1\*</sup>

5 Arjen P. Stroeven<sup>2,3</sup>

6 Nathaniel A. Lifton<sup>4,5</sup>

7 Jakob Heyman<sup>6</sup>

8 Alexander Lewerentz<sup>1</sup>

9 Kristina Hippe<sup>7</sup>

10 Jens-Ove Näslund<sup>8</sup>

11 Marc W. Caffee<sup>4,5</sup>

12

13 <sup>1</sup>Geological Survey of Sweden

14 <sup>2</sup>Department of Physical Geography, Stockholm University

15 <sup>3</sup>Bolin Centre for Climate Research, Stockholm University

16 <sup>4</sup>Department of Earth, Atmospheric, and Planetary Sciences, Purdue University

17 <sup>5</sup>Department of Physics and Astronomy, Purdue University

18 <sup>6</sup>Department of Earth Sciences, University of Gothenburg

19 <sup>7</sup>Umweltplanung Dr. Klimsa

20 <sup>8</sup>Swedish Nuclear Fuel and Waste Management Company (SKB)

21

22 \*Corresponding author: [bradley.goodfellow@sgu.se](mailto:bradley.goodfellow@sgu.se)

23

24 **Abstract**

25 *In situ* cosmogenic  $^{14}\text{C}$  (*in situ*  $^{14}\text{C}$ ) in quartz provides a recently developed tool to date exposure of  
26 bedrock surfaces up to ~25,000 years. From outcrops located in east-central Sweden, we test the  
27 accuracy of *in situ*  $^{14}\text{C}$  dating against (i) a relative sea level (RSL) curve constructed from radiocarbon  
28 dating of organic material in isolation basins, and (ii) the timing of local deglaciation constructed from  
29 a clay varve chronology complemented with traditional radiocarbon dating. Five samples of granitoid  
30 bedrock were taken along an elevation transect extending southwestwards from the Baltic Sea coast  
31 near Forsmark. Because these samples derive from bedrock outcrops positioned below the highest  
32 postglacial shoreline, they target the timing of progressive landscape emergence above sea level. In  
33 contrast, *in situ*  $^{14}\text{C}$  concentrations in an additional five samples taken from granitoid outcrops above  
34 the highest postglacial shoreline, located 100 km west of Forsmark, should reflect local deglaciation

35 ages. The ten *in situ*  $^{14}\text{C}$  measurements provide robust age constraints that, within uncertainties,  
36 compare favorably with the RSL curve and with the local deglaciation chronology. These data  
37 demonstrate the utility of *in situ*  $^{14}\text{C}$  to accurately date ice sheet deglaciation, and durations of  
38 postglacial exposure, in regions where cosmogenic  $^{10}\text{Be}$  and  $^{26}\text{Al}$  routinely return complex exposure  
39 results.

## 40 **1. Introduction**

41 The pacing of retreat of ice sheets in North America and Eurasia since their maximum expansion  
42 during the last glaciation remains an active research field (e.g., Hughes et al., 2016; Stroeven et al.,  
43 2016; Patton et al., 2017; Dalton et al., 2020, 2023). Understanding the triggers and processes causing  
44 the demise of these ephemeral ice sheets yields the best blueprint for understanding the future  
45 behavior of the Greenland and Antarctic ice sheets in a warming climate. Coupling the behavior of  
46 deglaciating ice sheets over the course of the Late Glacial and early Holocene to increasingly precise  
47 climate reconstructions, including climatic events, requires increased precision in ice sheet  
48 reconstructions (e.g., Bradwell et al., 2021). Precision can be enhanced through coupling  
49 geomorphological mapping of ice sheet margins (such as moraines, grounding zone wedges, lateral  
50 meltwater channels, and ice-dammed lake shorelines and spillways) with numerical field constraints  
51 from a diverse array of dating techniques (e.g., Stroeven et al., 2016; Bradwell et al., 2021; Regnéll et  
52 al., 2023).

53 Ice sheet reconstructions, especially in North America, have become highly detailed through  
54 radiocarbon dating (Dyke et al., 2002; Dalton et al., 2020). With the advance of offshore imaging of  
55 glacial geomorphology (Greenwood et al., 2017, 2021; Bradwell et al., 2021), radiocarbon dating has  
56 received a renewed upswing in recent years (e.g., Dalton et al., 2020; Bradwell et al., 2021). However,  
57 large landscape areas lack radiocarbon age constraints on ice sheet retreat because of an absence of  
58 datable organic material. Fortunately, optically stimulated luminescence ages on buried sand layers  
59 (e.g., Alexanderson et al., 2022) and cosmogenic nuclide apparent exposure ages on exposed bedrock  
60 and erratics have narrowed some of the gaps (e.g., Hughes et al., 2016; Stroeven et al., 2016; Dalton et  
61 al., 2023). In studies using cosmogenic nuclides, an ‘apparent’ exposure age is derived from a simple  
62 calculation from the nuclide concentration under consideration (Lal, 1991; Gosse and Phillips, 2001).  
63 Correctly interpreting the exposure age relies on modelling that considers geological factors that can  
64 reduce the nuclide concentration relative to the time since initial subaerial exposure (such as erosion  
65 and burial by glacial ice, water, snow, and/or soil; Gosse and Phillips, 2001; Schildgen et al., 2005; Ivy-  
66 Ochs and Kober, 2008). Exposure dating is the only technique available in regions where ice sheet  
67 erosion has left the surface bare or covered by a thin drape of till. Kleman et al. (2008) show that for  
68 Fennoscandia, these conditions are widespread in coastal regions where ice accelerated towards its

69 streaming sectors and where wave wash during glacial rebound further thinned or removed pre-  
70 existing sediment covers.

71 Coastal sectors in formerly glaciated regions provide sites important to the study of paleoglaciology.  
72 They offer an abundance of bedrock exposures from which patterns and processes of subglacial  
73 erosion can be studied through cosmogenic nuclide exposure dating (e.g., Hall et al., 2020). Also,  
74 because of the interplay with postglacial sea level, coastal areas yield data on glacioisostatic rebound  
75 that are critical to geodynamic modelling of Earth rheology and thicknesses of former ice sheets (e.g.,  
76 Lambeck et al. (1998, 2010) and Patton et al. (2017), for Fennoscandian examples). Geodynamic  
77 models require validation against measurements of vertical crustal motion (Steffen and Wu, 2011),  
78 such as those provided by recent global positioning system (GPS) measurements (e.g., Lidberg et al.,  
79 2010) and postglacial records of crustal rebound afforded by relative sea level (RSL) curves (e.g., Pålsson  
80 and Andersson, 2005). The construction of RSL curves, detailing the history of land surface emergence  
81 from sea level, is traditionally done using either sediments accumulated in isolation basins at different  
82 elevations above sea level or by dating uplifted gravel beach ridges. Typically, isolation basins, and their  
83 sediments, show a progression from marine, to brackish, and finally to freshwater environments as  
84 they are uplifted through tidal levels (Long et al., 2011). Histories of land uplift above sea level are  
85 documented using micro- and macrofossil analyses of isolation basin sediments and radiocarbon  
86 dating on macrofossils (Romundset et al., 2011). Uplifted beach ridges can be radiocarbon dated from  
87 a variety of materials (Blake, 1993) but most confidently from driftwood, whalebone, and shells (e.g.,  
88 Dyke et al., 1992). Gravel beach ridges have also been investigated using OSL and  $^{10}\text{Be}$  exposure dating  
89 even though, other than the highest beach ridge, they may be prone to clast reworking (Briner et al.,  
90 2006; Simkins et al., 2013; Bierman et al., 2018). A distinct advantage of constructing RSL curves using  
91 cosmogenic nuclides is that land surface emergence above sea level may be additionally dated from  
92 boulders (Briner et al., 2006) or bedrock (Bierman et al., 2018).

93 The potential for cosmogenic surface exposure dating of last ice sheet retreat in recently glaciated low-  
94 relief cratonic landscapes would seemingly be high because of the frequent outcropping of glacially  
95 sculpted quartz-bearing crystalline bedrock. However, the ice sheet may have been either non-erosive  
96 or erosion was insufficiently deep to remove all the cosmogenic nuclide inventory from previous  
97 exposure periods. Apparent ages are therefore often older than indicated by radiocarbon dating  
98 (Heyman et al., 2011; Stroeve et al., 2016) because they include a component of nuclide inheritance.  
99 Apparent ages younger than indicated by radiocarbon dating can also occur if sampled rock surfaces  
100 have been shielded, for example by sediments, following deglaciation. Concentrations of  $^{10}\text{Be}$  and  $^{26}\text{Al}$ ,  
101 in either bedrock or erratic boulders, often reflect complex exposure histories rather than simple  
102 deglacial exposure durations (Heyman et al., 2011; Stroeve et al., 2016).

103 In this study we use  $^{14}\text{C}$  produced *in situ* in quartz-bearing bedrock (*in situ*  $^{14}\text{C}$ ) because it potentially  
104 circumvents an overt reliance on the need for deep erosion (>3 m) to remove the inherited signal from  
105 previous exposure periods (Gosse and Phillips, 2001). Because of its short half-life of  $5700 \pm 30$  years,  
106 inherited *in situ*  $^{14}\text{C}$  will decay if ice sheet burial at investigated sites during the last glacial phase  
107 (marine isotope stage 2; MIS2) exceeded 25-30 ka, that is, ca. 5 half-lives (Briner et al., 2014).

108 Some studies assessing changes in glacier and ice sheet extents over Late Glacial to Holocene  
109 timescales have used *in situ*  $^{14}\text{C}$  (Miller et al., 2006; Fogwill et al., 2014; Hippe et al., 2014;  
110 Schweinsberg et al., 2018; Pendleton et al., 2019; Young et al., 2021; Schimmelpfennig et al., 2022). In  
111 these studies, *in situ*  $^{14}\text{C}$  has been applied with other nuclides with longer half-lives, in particular  $^{10}\text{Be}$ ,  
112 to unravel complex histories of glacier advance and retreat (e.g., Goehring et al., 2011) and spatial  
113 patterns in glacial erosion in mountainous terrain (e.g., Steinemann et al., 2021). Extensive regions  
114 formerly covered by ice sheets are characterized by low relief and low elevation terrain. The  
115 effectiveness of *in situ*  $^{14}\text{C}$  in dating ice sheet retreat in these non-alpine settings and in quantifying  
116 shoreline displacement from bedrock samples has not been previously assessed. The aim of this study  
117 is therefore to validate the use of  $^{14}\text{C}$  formed *in situ* in bedrock as a reliable chronometer by evaluating  
118 its performance in duplicating (i) a previously-established Holocene RSL curve based on radiocarbon  
119 dating (Hedenström and Risberg, 2003; SKB, 2020) and (ii) the timing of deglaciation above the highest  
120 (post-glacial) shoreline in nearby east-central Sweden according to reconstructions of deglaciation of  
121 the last ice sheet (Hughes et al., 2016; Stroeven et al., 2016).

122

## 123 **2. Study Area**

124 Our study is focused on a region that includes low elevation, low relief, Forsmark-Uppland and  
125 adjoining higher elevation and relief Dalarna-Gävleborg in east-central Sweden (Fig. 1). This region was  
126 selected because Forsmark is the location of a planned geological repository for spent nuclear fuel  
127 (e.g., SKB 2022). As such, this region has been intensively studied and has a wealth of geologic data  
128 relevant to our study. This includes in-depth analyses of bedrock and environmental properties,  
129 including influences of glacial and postglacial processes (e.g., Lönnqvist and Hökmark, 2013; Hall et al.,  
130 2019; Moon et al., 2020; SKB, 2020).

131 From spatio-temporal ice sheet reconstructions by Kleman et al. (2008), the study area was glaciated  
132 16-20 times for a total duration of c. 330 kyr over the past 1 Ma. The last deglaciation of the study area  
133 is well-constrained by two recent reconstructions that differ in their approach (Hughes et al., 2016;  
134 Stroeven et al., 2016). The Hughes et al. (2016) reconstruction relies primarily upon chronological  
135 constraints supplied from radiocarbon, thermal luminescence, optically stimulated luminescence  
136 (OSL), infrared stimulated luminescence, electron spin resonance, terrestrial cosmogenic nuclide

137 (TCN), and U-series dating. Published landform data, mostly with respect to end moraines and  
138 generally accepted correlations of ice-margin positions between individual moraines, provide  
139 complementary evidence. In contrast, the Stroeven et al. (2016) reconstruction combines  
140 geomorphological constraints for ice sheet margin outlines, including ice-marginal depositional  
141 landforms and meltwater channels, ice-dammed lakes, eskers, lineations, and striae, with  
142 chronological constraints supplied by radiocarbon, varve, OSL, and TCN dating. Whereas Hughes et al.  
143 (2016) reconstruct ice sheet retreat every 1 ka, and for every ice margin plot its position as “most  
144 credible”, “min”, and “max”, Stroeven et al. (2016) present ice margin positions for every 100 years  
145 inside the Younger Dryas standstill position (Stroeven et al., 2015). These marginal positions are  
146 temporally and spatially defined by the “Swedish Time Scale” clay varve record along the Swedish east  
147 coast (De Geer, 1935, 1940; Strömberg, 1989, 1994; Brunnberg, 1995; Wohlfarth et al., 1995). From  
148 Stroeven et al. (2016), the last deglaciation of the study area occurred  $10.8 \pm 0.3$  ka BP, which overlaps  
149 the timing of deglaciation of the study area from Hughes et al. (2016), within uncertainty (Fig. 1). The  
150 highest postglacial shoreline in east-central Sweden is located at a present elevation of  $\sim 200$  m a.s.l. in  
151 Dalarna-Gävleborg,  $\sim 100$  km west of Forsmark (SGU, 2015). The exposure duration of bedrock above  
152 the highest postglacial shoreline represents the time since local deglaciation. Hence, *in situ*  $^{14}\text{C}$  ages  
153 from bedrock above the highest postglacial shoreline should conform to the reconstructed  
154 deglaciation age of  $10.8 \pm 0.3$  ka from Stroeven et al. (2016).

155 Below the highest postglacial shoreline, in the Forsmark-Uppland region, the last deglaciation  
156 occurred in a marine environment and the landscape has progressively emerged above sea level  
157 through postglacial isostatic uplift. A RSL curve constructed from radiocarbon dating of basal organic  
158 sediments trapped in isolation basins along elevation transects describes the progressive emergence  
159 of the Forsmark-Uppland landscape above sea level (Robertsson and Persson, 1989; Risberg, 1999;  
160 Bergström, 2001; Hedenström and Risberg, 2003; Berglund, 2005; SKB, 2020). Ages calculated from *in*  
161 *situ*  $^{14}\text{C}$  from bedrock outcrops along an elevation transect would then mirror the Forsmark RSL curve  
162 for their corresponding elevations (but be slightly older because of nuclide production through  
163 shallow water before emergence).

164 A potential complication to the accurate exposure age dating of bedrock surfaces using *in situ*  $^{14}\text{C}$  in  
165 east-central Sweden is that the most recent period of ice sheet burial may not have been sufficiently  
166 long to decay any *in situ*  $^{14}\text{C}$  inventory inherited from prior exposure. Here, the extent of the  
167 Fennoscandian Ice Sheet during interstadial MIS3 and the timing of ice advance across the Forsmark  
168 region during late MIS3 are crucially important. Kleman et al. (2020) have identified ice-free conditions  
169 around Idre (330 km NW, up-ice, of our study area; Fig. 1) between 55 ka and 35 ka, which implies  
170 inundation of our study area by ice after 35 ka. Combined with a well-constrained final deglaciation  
171 age of  $10.8 \pm 0.3$  ka (Stroeven et al. 2016), it appears that our study area has most recently (during

172 MIS2) been inundated by glacial ice for at most 24 ka. This inference is in line with results from ice  
173 sheet modelling indicating a 22 kyr duration of ice-cover at Forsmark during MIS2 (SKB, 2020).  
174 Consequently, it is possible that *in situ*  $^{14}\text{C}$  concentrations may reflect subaerial exposure of bedrock in  
175 our study area during MIS3 in addition to Holocene exposure, resulting in an offset towards older ages  
176 relative to the RSL curve for Forsmark (Hedenström and Risberg, 2003; SKB, 2020) and the deglaciation  
177 chronologies of Hughes et al. (2016) and Stroeven et al. (2016).

178

### 179 3. Methods

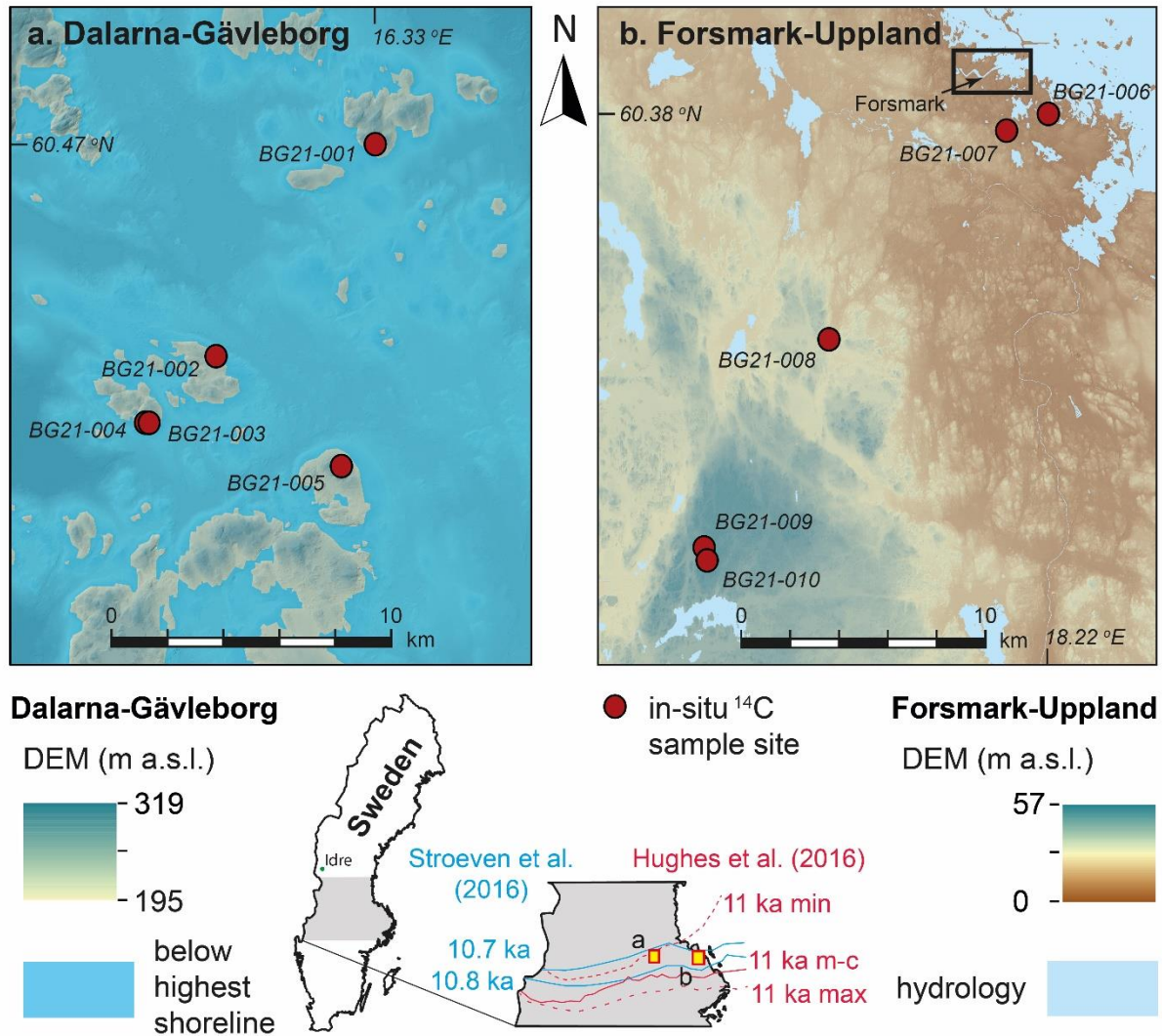
#### 180 3.1. Sampling of bedrock outcrops for *in situ* $^{14}\text{C}$ measurement

181 We used the following sampling strategy to evaluate the accuracy of bedrock exposure ages derived  
182 from *in situ*  $^{14}\text{C}$  against the Forsmark RSL curve and the deglaciation of the last ice sheet in east-central  
183 Sweden. A rigorous scheme was applied to ensure that we avoided sampling quartz altered through  
184 hydrothermal processes that is likely to occur in major pegmatite intrusions, outcrops located in major  
185 deformation zones, and outcrop-scale veins, fractures, and adjacent rock volumes. Consequently,  
186 sampling was done on outcrops of metagranitoid from the early-Svecokarelian GDG-GSDG suite that  
187 dominates the Bergslagen lithotectonic unit (Stephens and Jansson, 2020). A petrological examination  
188 using transmitted light polarization microscopy was applied to thin sections to ascertain that the quartz  
189 was unlikely to contain multi-fluid phase, vapour phase, or solid-phase inclusions. All samples were  
190 collected using an angle grinder, which permits sampling of hard crystalline bedrock isolated from  
191 outcrop edges, fractures, and quartz veins, and consistently limits sample thicknesses to 3 cm.

192 We collected a total of ten samples for *in situ*  $^{14}\text{C}$  analyses. Five of these were collected along a SW-NE  
193 transect near Forsmark (Fig. 1b). These outcrops were chosen because they span an elevation gradient  
194 of 9.4–56.0 m a.s.l. and exposure ages derived from *in situ*  $^{14}\text{C}$  can therefore be evaluated against the  
195 Forsmark RSL curve. We collected a further five samples from locations above the highest shoreline (Fig.  
196 1a) to determine the age of local deglaciation for comparison with published deglaciation chronologies  
197 (Hughes et al., 2016; Stroeven et al., 2016). Sample locations were logged on a 2 m-resolution LiDAR  
198 digital elevation model (DEM) displayed in ArcGIS 10 on a tablet computer. A GPS add-in tool in ArcGIS  
199 10 was used to record positional data, within a horizontal precision of 2 m. The elevation of each sample  
200 location was extracted from the DEM and has a precision of tens of centimetres. The influence of these  
201 minor positional uncertainties on our  $^{14}\text{C}$  calculations is trivial and none of the sample sites is influenced  
202 by topographic shielding that could reduce the accumulation of  $^{14}\text{C}$  in bedrock.

203 Each sampled bedrock outcrop formed a local topographic high, which minimizes the risk of burial by  
204 soil and snow (Supplement 1). Moss mats were present on all sampled outcrops. Although we avoided

205 sampling bedrock that was moss-covered, we cannot be certain that moss mats did not formerly cover  
 206 the sample sites. Given a compressed thickness of 0.5 cm and an estimated density of  $0.7 \text{ g cm}^{-3}$ , this  
 207 may have contributed to a shielding of the sampled rock surfaces of  $0.35 \text{ g cm}^{-2}$ , which is negligible and  
 208 is therefore excluded from our age inferences.



209  
 210 **Figure 1.** Sample locations for *in situ*  $^{14}\text{C}$  dating in **(a)** Dalarna-Gävleborg and **(b)** Forsmark-Uppland. The  
 211 five Dalarna-Gävleborg sample sites are located on what were islands above the highest postglacial  
 212 shoreline (shown), whereas the five sample sites from Forsmark-Uppland are located below the highest  
 213 shoreline (not shown because the entire area was submerged). See inset maps for locations of panels a  
 214 and b and for the 10.7 ka BP and 10.8 ka BP retreat isochrones (blue) from Stroeven et al. (2016) and 11  
 215 ka BP (most-credible, minimum, and maximum) retreat isochrones (red) from Hughes et al. (2016). The  
 216 rectangle in panel b approximately indicates the site selected for the planned geological repository for  
 217 spent nuclear fuel at Forsmark. DEM with 2 m resolution, from LiDAR data, Lantmäteriet.

### 218 **3.2. Laboratory preparation for accelerator mass spectrometry (AMS)**

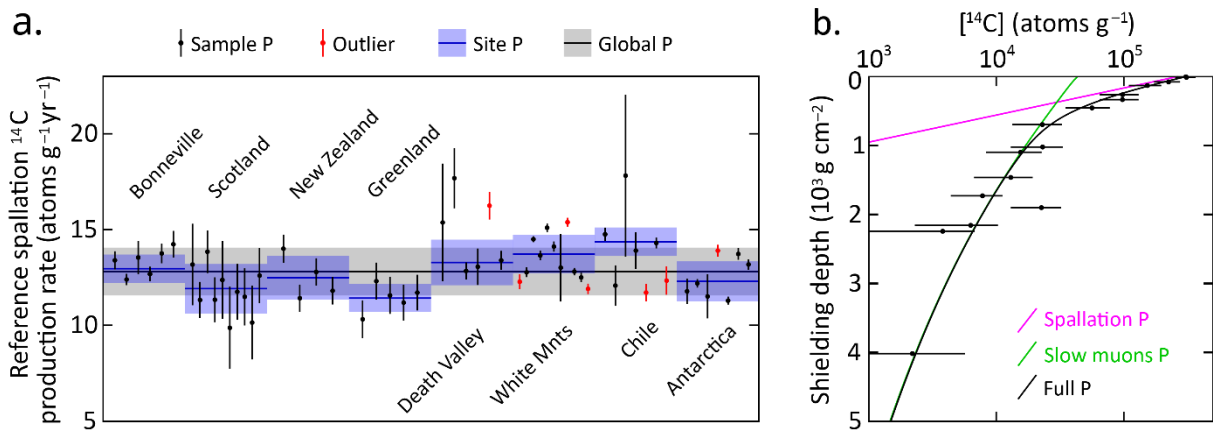
219 Samples were physically and chemically processed at the Purdue Rare Isotope Measurement Laboratory  
220 (PRIME Lab) at Purdue University, U.S.A. Concentrations of *in situ*  $^{14}\text{C}$  were determined from purified  
221 quartz separates through automated procedures (Lifton et al., 2023). Approximately 5 g of quartz from  
222 each sample was added to a degassed  $\text{LiBO}_2$  flux in a re-usable 90% Pt/10% Rh sample boat and heated  
223 to 500 °C for one hour in ca. 6.7 kPa of Research Purity  $\text{O}_2$  to remove atmospheric contaminants, which  
224 were discarded. The sample was then heated to 1100 °C for three hours to dissolve the quartz and  
225 release the *in situ*  $^{14}\text{C}$ , again in an atmosphere of ca. 6.7 kPa of Research Purity  $\text{O}_2$  to oxidize any evolved  
226 carbon species to  $\text{CO}_2$ . The  $\text{CO}_2$  from the 1100 °C step was then purified, measured quantitatively, and  
227 converted to graphite for  $^{14}\text{C}$  AMS measurement at PRIME Lab (Lifton et al., 2023). To test for data  
228 reproducibility, sample BG21-002 was randomly selected to undergo laboratory preparation and AMS a  
229 second time. Measured concentrations of *in situ*  $^{14}\text{C}$  are calculated from the measured isotope ratios via  
230 AMS following Hippe and Lifton (2014) (Table 1).

### 231 **3.3. Exposure age calculations**

232 The expage calculator version 202403 (<http://expage.github.io/calculator>) is used to calculate apparent  
233 exposure ages. It is based on the original CRONUS calculator v. 2 (Balco et al., 2008), the LSDn production  
234 rate scaling (Lifton et al., 2014), and the CRONUScalc calculator (Marrero et al., 2016), using the  
235 geomagnetic framework of Lifton (2016) with the SHA.DIF.14k model for the last 14 kyr. Exposure ages  
236 are calculated using resulting time-varying  $^{14}\text{C}$  production rates accounting for decay and interpolated  
237 to match the measured  $^{14}\text{C}$  concentration. The production rate from muons is calibrated against the  
238 Leymon High core  $^{14}\text{C}$  data of Lupker et al. (2015) and the production rate from spallation is calibrated  
239 against updated global  $^{14}\text{C}$  production rate calibration data (Schimmelpfennig et al., 2012; Young et al.,  
240 2014; Lifton et al., 2015; Borchers et al., 2016; Phillips et al., 2016; Koester and Lifton, 2023, corrigendum  
241 in prep). This calibration is done iteratively for spallation and muons to reach convergence, using the  
242 expage production rate calibration methods (Fig. 2).

243 Exposure age calculations along the Forsmark-Uppland transect account for  $^{14}\text{C}$  production during  
244 emergence through shallow water. Burial of sampled surfaces by snow is excluded from the age  
245 calculations for all sample sites because we neither know how snow burial depths and durations vary  
246 between sites nor vary through time. The effect of snow burial would be to slightly decrease cosmogenic  
247 nuclide production in the underlying rock surface (Schildgen et al., 2005) and we have minimized this  
248 effect through our sampling strategy.





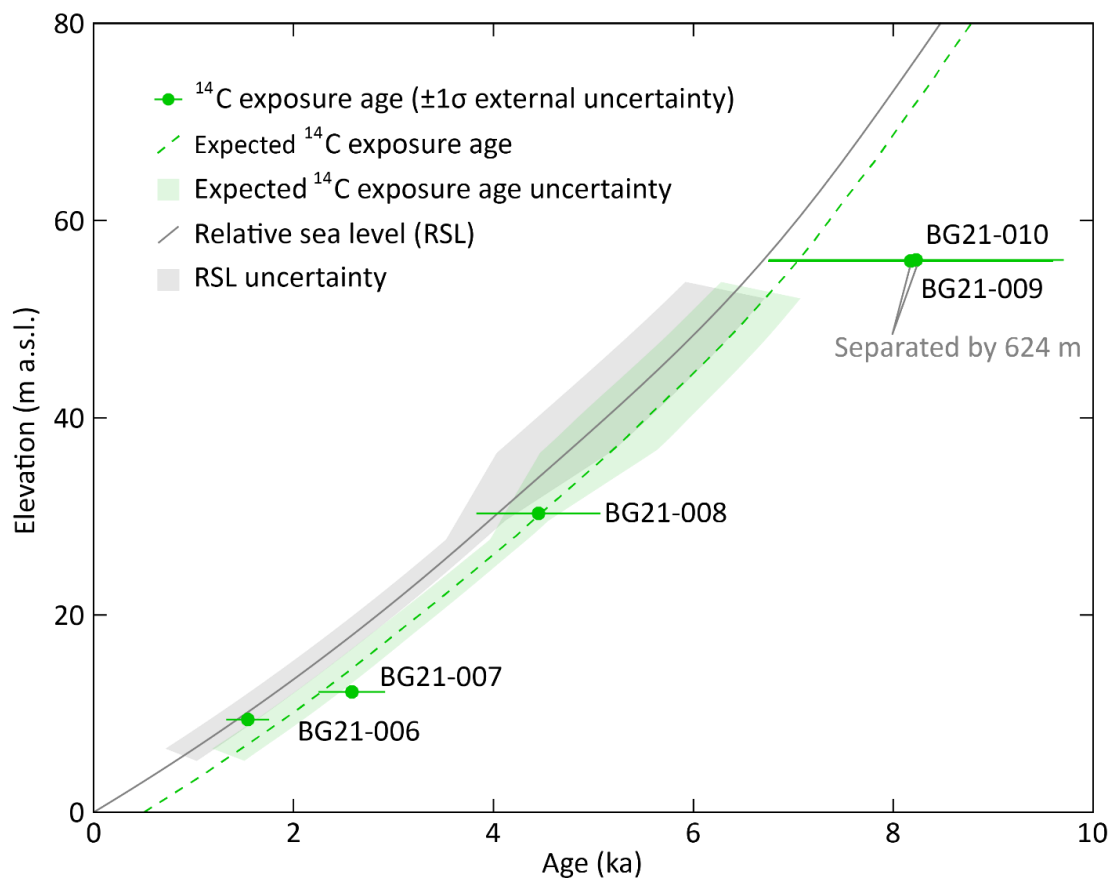
249 **Figure 2.** Production rate calibration of  $^{14}\text{C}$  in quartz. **(a)** Reference spallation  $^{14}\text{C}$  production rate  
 250 calibration based on data from Schimmelpfennig et al. (2012), Young et al. (2014), Lifton et al. (2015),  
 251 Borchers et al. (2016), and Phillips et al. (2016), corrected per Hippe and Lifton (2014) and compiled in  
 252 Koester and Lifton (2023). An uncertainty-weighted production rate is calculated for each of the eight  
 253 sites. Outliers, which are not included in the uncertainty-weighted production rates, are determined  
 254 based on the requirement that there should be at least three samples yielding a reduced chi-square  
 255 statistic ( $X_R^2$ ) with a p-value of at least 0.05 for the assumption that the individual production rates from  
 256 a site are derived from one normal distribution. For  $X_R^2$ , but not the uncertainty-weighting, we use the  
 257 largest of the sample-specific production rate uncertainty based on the  $^{14}\text{C}$  concentration uncertainties  
 258 and 5% of the sample production rate. This procedure does not punish samples with low measurement  
 259 uncertainties, which otherwise risk exclusion as outliers. We adopt a global reference spallation  $^{14}\text{C}$   
 260 production rate of  $12.81 \pm 1.25$  atoms  $\text{g}^{-1} \text{yr}^{-1}$ , calculated as the arithmetic mean of the eight site  
 261 production rates with the uncertainty being based on an uncertainty-weighted deviation of all included  
 262 single sample production rates, excluding outliers. **(b)** Calibration of  $^{14}\text{C}$  production rate from muons  
 263 based on the data of Lupker et al. (2015). The calibration is based on the method used in the CRONUScal  
 264 calculator (Marrero et al., 2016; Phillips et al., 2016). The figure shows the best fit  $^{14}\text{C}$  concentration  
 265 profiles produced from spallation, slow muons, and full production. The best fit yields near zero  
 266 production from fast muons (cf. Lupker et al., 2015). The production rate calibration has been carried  
 267 out using the expage-202403 calculator in an iterative way to make the global reference spallation  $^{14}\text{C}$   
 268 production rate converge with the production rate from muons.

269

## 270 4. Results

271 Analytical results for *in situ*  $^{14}\text{C}$  samples and procedural blanks are presented in Table 1. The mean and  
 272 standard deviation are used to correct measured  $^{14}\text{C}$  sample inventories (Table 1) because procedural  
 273 blanks are well-constrained during the analytical time frame. Inferred ages for the five *in situ*  $^{14}\text{C}$  samples  
 274 from the Forsmark-Uppland transect (i.e., below the highest postglacial shoreline) are shown relative to

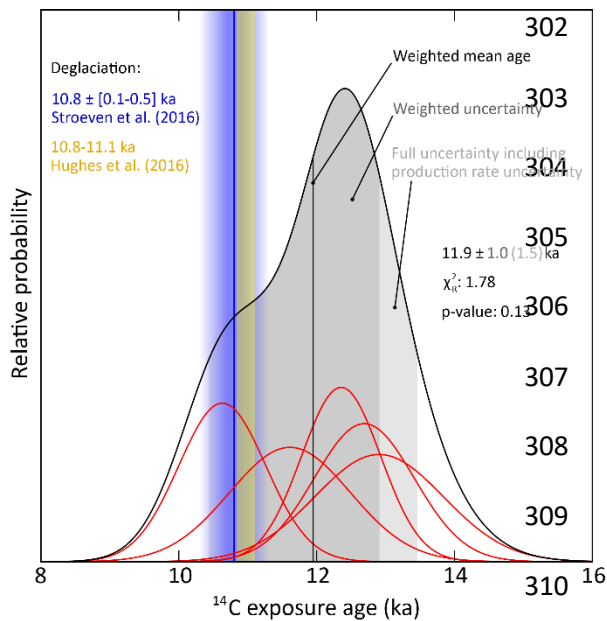
275 the Holocene RSL curve for Forsmark and the expected *in situ*  $^{14}\text{C}$  exposure age curve considering  
 276 subaqueous cosmogenic nuclide production (Figure 3; Table 2). Exposure age uncertainties are large  
 277 with internal uncertainties (measurement uncertainties; Balco et al., 2008) of 5-9% and external  
 278 uncertainties of 13-25% (also including production rate uncertainties, which are high relative to  $^{10}\text{Be}$   
 279 (Borchers et al., 2016; Phillips et al., 2016). Apparent exposure ages increase consistently with elevation  
 280 and match expected ages within uncertainty. The two highest samples have near-identical apparent  
 281 exposure ages and elevations. However, these samples provide independent ages because they are  
 282 horizontally separated by 624 m (Figure 1b). There is good agreement between ages inferred from these  
 283 *in situ*  $^{14}\text{C}$  data and the RSL curve constructed from organic radiocarbon dating of isolation events  
 284 (Hedenström and Risberg, 2003; SKB, 2020).



285

286 **Figure 3.** Apparent  $^{14}\text{C}$  exposure ages for five Forsmark samples from below the highest shoreline (Fig.  
 287 1b; Table 2) with  $1\sigma$  external uncertainties. The expected exposure ages are calculated assuming the RSL  
 288 curve is correct, the  $^{14}\text{C}$  spallation production rate is correct, partial exposure as the sample approaches  
 289 the water surface, and full post-glacial exposure for the duration above sea level. Hence, the expected  
 290 exposure age curve is a few hundred years older than the RSL curve. The RSL curve is from SKB (2020)  
 291 and uncertainties for the 1–6 ka interval are calculated from the original radiocarbon data in Hedenström  
 292 and Risberg (2003). The RSL uncertainty envelope is also transposed onto the expected exposure age  
 293 curve.

294 Apparent exposure ages for the five *in situ*  $^{14}\text{C}$  samples located above the highest shoreline in Dalarna  
 295 and Gävleborg (Fig. 1a) are shown in Figure 4 and Table 2. The weighted mean age from all five samples  
 296 is  $11.9 \pm 1.5$  ka. These data display a  $\chi^2_R$  of 1.78 and a p-value of 0.13 based on  $1\sigma$  internal uncertainties,  
 297 which does not support a rejection of the hypothesis that the apparent exposure ages represent the  
 298 same population. In addition to the samples being from the same population, the exposure ages are  
 299 consistent, within uncertainty, with the expected deglaciation age of  $10.8 \pm 0.3$  ka (Stroeven et al. 2016).  
 300 Replicate measurements on sample BG21-002 closely agree and an age based on a weighted mean  $^{14}\text{C}$   
 301 concentration is shown in Figure 4.



311 **Figure 4.** Normalized kernel density estimates of the exposure ages from samples above the highest  
 312 shoreline (Fig. 1a; Table 2). The individual samples (red curves) display  $1\sigma$  internal uncertainty  
 313 (measurement uncertainty). For the repeat sample BG21-002, the exposure age is calculated with a  
 314 weighted mean  $^{14}\text{C}$  concentration using a 2% uncertainty. The cosmogenic nuclide ages yield a reduced  
 315 chi-square ( $\chi^2_R$ ) of 1.78 and a p-value of 0.13 based on internal uncertainties, which indicates that they  
 316 are from the same population.

**Table 1. *In situ* <sup>14</sup>C sample measurement details**

Sample	PCEGS <sup>1</sup> #	PLID <sup>2</sup>	Mass Quartz (g)	C yield (μg)	Diluted Mass C (μg)	AMS Split Mass C <sup>3</sup> (μg)	δ <sup>13</sup> C (‰ VPDB <sup>4</sup> )	<sup>14</sup> C/ <sup>13</sup> C <sup>5</sup> (10 <sup>-12</sup> )	<sup>14</sup> C/C <sub>total</sub> <sup>6</sup> (10 <sup>-14</sup> )	<sup>14</sup> C <sup>7</sup> (10 <sup>5</sup> at)	[ <sup>14</sup> C] (10 <sup>5</sup> at g <sup>-1</sup> )
BG21-001	PCEGS-146	202101960	5.02378	5.0 ± 0.1	393.8 ± 4.8	382.3 ± 4.6	-45.9 ± 0.2	3.3992 ± 0.0745	3.4118 ± 0.0785	6.1771 ± 0.1793	1.2296 ± 0.0357
BG21-002	PCEGS-147	202101961	5.02383	7.8 ± 0.1	303.3 ± 3.7	294.4 ± 3.6	-44.8 ± 0.2	4.5548 ± 0.0964	4.6226 ± 0.1016	6.4703 ± 0.1806	1.2879 ± 0.0360
BG21-002R	PCEGS-150	202201473	5.04116	7.7 ± 0.1	305.3 ± 3.7	296.4 ± 3.6	-45.2 ± 0.2	4.5575 ± 0.1350	4.6239 ± 0.1422	6.5186 ± 0.2368	1.2931 ± 0.0470
BG21-003	PCEGS-148	202101962	5.01070	17.6 ± 0.3	303.4 ± 3.7	294.5 ± 3.6	-43.9 ± 0.2	4.6325 ± 0.1075	4.7091 ± 0.1134	6.6042 ± 0.1969	1.3180 ± 0.0393
BG21-004	PCEGS-152	202101963	5.05927	11.9 ± 0.2	305.7 ± 3.7	296.8 ± 3.6	-44.6 ± 0.2	4.6181 ± 0.0789	4.6905 ± 0.0832	6.6300 ± 0.1588	1.3105 ± 0.0314
BG21-005	PCEGS-153	202101964	5.07578	4.6 ± 0.1	304.5 ± 3.7	295.6 ± 3.6	-45.4 ± 0.2	4.5997 ± 0.1272	4.6668 ± 0.1339	6.5656 ± 0.2251	1.2935 ± 0.0444
BG21-006	PCEGS-155	202101965	5.06572	5.5 ± 0.1	306.8 ± 3.7	297.8 ± 3.6	-45.2 ± 0.2	1.2766 ± 0.0562	1.1715 ± 0.0594	1.2426 ± 0.1010	0.2453 ± 0.0199
BG21-007	PCEGS-157	202101966	5.03589	6.9 ± 0.1	309.2 ± 3.8	300.1 ± 3.7	-45.0 ± 0.2	1.6838 ± 0.0507	1.6007 ± 0.0536	1.9221 ± 0.0960	0.3817 ± 0.0191
BG21-008	PCEGS-158	202101967	5.07653	4.0 ± 0.1	308.9 ± 3.8	299.9 ± 3.6	-45.4 ± 0.2	2.3565 ± 0.0634	2.3076 ± 0.0669	3.0145 ± 0.1185	0.5938 ± 0.0234
BG21-009	PCEGS-160	202101968	5.01906	55.3 ± 0.7	305.6 ± 3.7	296.6 ± 3.6	-38.0 ± 0.2	3.3393 ± 0.0946	3.3681 ± 0.1005	4.6013 ± 0.1703	0.9168 ± 0.0339
BG21-010	PCEGS-161	202101969	4.99961	42.2 ± 0.6	306.0 ± 3.7	297.0 ± 3.6	-40.1 ± 0.2	3.3197 ± 0.0680	3.3399 ± 0.0721	4.5648 ± 0.1321	0.9130 ± 0.0264
<b>Procedural Blanks</b>											
PB2-03222022	PCEGS-135	202201450	--	1.4 ± 0.1	305.2 ± 3.7	296.2 ± 3.6	-40.2 ± 0.2	0.4853 ± 0.0298	0.3413 ± 0.0320	0.5222 ± 0.0493	--
PB2-04212022	PCEGS-145	202201452	--	1.8 ± 0.1	307.0 ± 3.7	298.0 ± 3.6	-46.0 ± 0.2	0.5182 ± 0.0273	0.3731 ± 0.0292	0.5742 ± 0.0455	--
PB2-05212022	PCEGS-163	202201454	--	2.3 ± 0.1	307.4 ± 3.7	298.4 ± 3.6	-46.0 ± 0.2	0.5364 ± 0.0315	0.3922 ± 0.0335	0.6045 ± 0.0521	--
PB2-06022022	PCEGS-169	202201459	--	2.3 ± 0.1	307.3 ± 3.7	298.3 ± 3.6	-40.3 ± 0.2	0.4920 ± 0.0291	0.3486 ± 0.0312	0.5371 ± 0.0486	--
								<u>Mean ± 1σ (All blanks)</u>		<u>0.5595 ± 0.0371</u>	
								<u>Mean ± 1σ (145, 163 only)</u>		<u>0.5894 ± 0.0214</u>	

**Notes**

- Purdue Carbon Extraction and Graphitization System.
- Prime Lab ID.
- Mass graphitized for AMS analysis after small aliquot (ca. 9 μg C) taken for stable C isotopic analysis offline.
- VPDB is Vienna Pee Dee Belemnite.
- Measured relative to OX-2 standard.
- Corrected for mass-dependent graphitization blank (based on AMS Split Mass C) and stable C composition.
- Sample values calculated using Diluted Mass C and corrected for mean procedural blank (All blanks).

Table 2. Apparent *in situ*  $^{14}\text{C}$  ages from quartz, Dalarna-Gävleborg and Forsmark-Uppland.

Sample <sup>1</sup>	Lat (°)	Long (°)	Elevation (m a.s.l.)	$^{14}\text{C}$ age <sup>2</sup> (ka)
<b>BG21-001</b>	60.47432	16.33134	236.5	10.6 ± 2.2 (± 0.6)
<b>BG21-002</b>	60.40615	16.22197	212.6	12.3 ± 2.9 (± 0.8)
<b>BG21-002R</b>	60.40615	16.22197	212.6	12.4 ± 3.0 (± 1.1)
<b>BG21-003</b>	60.38459	16.17649	216.3	12.9 ± 3.2 (± 0.9)
<b>BG21-004</b>	60.38451	16.17440	217.8	12.7 ± 3.0 (± 0.7)
<b>BG21-005</b>	60.36888	16.30526	248.1	11.6 ± 2.6 (± 0.9)
<b>BG21-006</b>	60.38490	18.22308	9.4	1.5 ± 0.2 (± 0.1)
<b>BG21-007</b>	60.37892	18.19129	12.2	2.6 ± 0.3 (± 0.2)
<b>BG21-008</b>	60.30504	18.04993	30.3	4.5 ± 0.6 (± 0.2)
<b>BG21-009</b>	60.22988	17.94989	56.0	8.2 ± 1.5 (± 0.5)
<b>BG21-010</b>	60.22431	17.95051	55.9	8.2 ± 1.4 (± 0.4)

## Notes

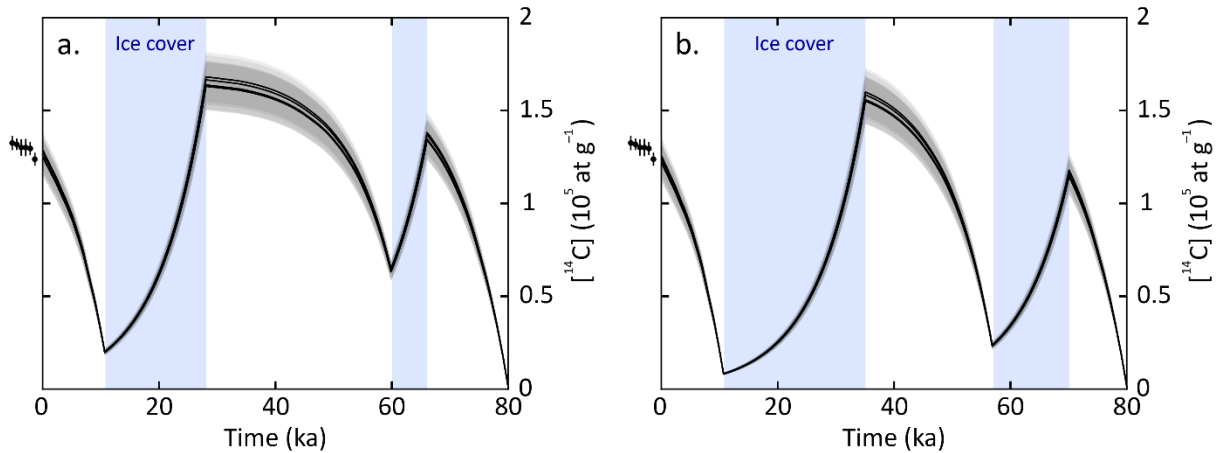
- 1 All samples have a thickness of 3 cm, a density of 2.7 g cm<sup>-3</sup>, and a shielding factor of 1. Zero erosion is assumed.
- 2  $^{14}\text{C}$  age and 1 $\sigma$  external uncertainty (1 $\sigma$  internal uncertainty).

## 321 5. Discussion

322 The *in situ*  $^{14}\text{C}$  bedrock exposure ages from the Forsmark-Uppland transect (i.e., below the highest  
323 postglacial shoreline) consistently increase with elevation and overlap the expected exposure age  
324 curve, within uncertainty (Fig. 3). This study adds to precious few applications of cosmogenic nuclides  
325 to defining postglacial landscape emergence above sea level (Briner et al., 2006; Bierman et al., 2018).  
326 Briner et al. (2006) present good (visual) congruence with a record of shoreline emergence built from  
327 radiocarbon-dated driftwood and fauna by Dyke et al. (1992) using  $^{10}\text{Be}$  measurements on boulders in  
328 beaches derived from wave-washed till. Their study also mentions that building a relative sea level  
329 curve from pebbles, cobbles and plucked bedrock suffered from inheritance problems, an experience  
330 shared by Matmon et al. (2003) while attempting the dating of chert on beach ridges in southern Israel  
331 and heeded by Bierman et al. (2018). Bierman et al. (2018) successfully dated landscape emergence on  
332 Greenland using  $^{10}\text{Be}$  across a range of settings, including bedrock below the highest shoreline, cobbles  
333 from beach ridges at the highest shoreline, and boulders and bedrock above the highest shoreline.  
334 They note that success hinges on the requirement of warm-based ice and deep glacial erosion in  
335 exposing bedrock devoid of an inherited cosmogenic nuclide inventory. In many regions, however,  
336 including east-central Sweden and more widely in Fennoscandia, these requirements are not met  
337 either because of cold-based conditions (Patton et al., 2016; Stroeven et al., 2016) or weakly erosive  
338 warm-based ice such as at Forsmark (Hall et al., 2019; SKB, 2020), during all or much of glacial time.  
339 Cosmogenic nuclide inheritance is therefore a part of the landscape fabric. Bierman et al. (2018)  
340 advocate the use of *in situ*  $^{14}\text{C}$  as a methodology to circumvent inheritance problems. Our study is the  
341 first to follow-up on that suggestion, and shows, convincingly, that using *in situ*  $^{14}\text{C}$  can extend the study  
342 of landscape rebound to regions where ice sheet erosion was insufficiently deep to allow for the  
343 application of long-lived nuclides.

344 Five bedrock samples from above the highest postglacial shoreline are well-clustered and the weighted  
345 mean age (and full uncertainty) of  $11.9 \pm 1.5$  ka overlaps with the predicted deglaciation age of  $10.8 \pm$   
346  $0.3$  ka (Fig. 4; Hughes et al., 2016; Stroeven et al., 2016). Because derived exposure ages overlap with  
347 the predicted deglaciation age, we further infer that the *in situ*  $^{14}\text{C}$  samples, including those located  
348 below the highest postglacial shoreline, within uncertainty, lack significant inheritance from previous  
349 exposure. Model scenarios of *in situ*  $^{14}\text{C}$  concentration evolution over varying durations of MIS2 and  
350 MIS4 ice cover are consistent with minor inheritance, even with short periods of ice coverage and no  
351 glacial or interglacial erosion (Figure 5). Even if the last ice sheet had advanced over the region as late

352 as 28 ka BP, there would only be a negligible inventory of inherited  $^{14}\text{C}$  atoms produced prior to the  
353 MIS2 ice advance.



354 **Figure 5.** Modelled *in situ*  $^{14}\text{C}$  concentration evolution over the last 80 kyr in the five samples (BG21-  
355 001– BG21-005) from above the highest shoreline. The  $^{14}\text{C}$  development is modelled assuming no  
356 glacial or interglacial erosion, continuous exposure to cosmic rays during ice-free periods, and full  
357 shielding from cosmic rays (no  $^{14}\text{C}$  production) during periods with ice cover. The points just left of the  
358 plots display the measured  $^{14}\text{C}$  concentrations for the six sample measurements (Table 1). (a) Scenario  
359 with short periods of MIS4 and MIS2 ice cover from 66 to 60 ka BP and from 28 ka BP to deglaciation  
360 around 10.7 ka BP. (b) Scenario with longer periods of MIS4 and MIS2 ice cover from 70 to 57 ka BP and  
361 from 35 ka BP to the deglaciation around 10.7 ka BP. Due to the rapid decay of  $^{14}\text{C}$  (half-life of  $5700 \pm$   
362  $30$  years), both scenarios yield similar end-point concentrations of  $^{14}\text{C}$  that overlap, within  
363 uncertainties, the measured sample concentrations.

364 Our *in situ*  $^{14}\text{C}$  data from above the highest (postglacial) shoreline demonstrate their potential for  
365 constraining the deglaciation chronology of former ice sheets. This is especially true for regions with  
366 thin till drapes, abundant bedrock exposures, and sparse moraines outlining successive retreat stages.  
367 In Fennoscandia, thin tills occur commonly (cf. Kleman et al., 2008) and ice sheet retreat appears to  
368 have proceeded uninterrupted inside the Younger Dryas moraine belt (apart from the Central Finland  
369 Ice-Marginal Formation; e.g., Rainio et al., 1986; Stroeven et al., 2016). Whereas the post-Younger  
370 Dryas deglaciation of east-central Sweden is well constrained by clay-varve chronology below the  
371 highest postglacial shoreline (Strömberg, 1989), there are vast areas above the highest shoreline that  
372 remain poorly constrained by data (Stroeven et al. 2016). In addition to a lack of datable deglacial  
373 landforms, this is attributable to glacial erosion of bedrock having frequently been insufficient to  
374 remove inventories of long half-life  $^{10}\text{Be}$  and  $^{26}\text{Al}$  (Patton et al., 2022), thereby leaving nuclides inherited  
375 from exposure prior to the last glaciation (Heyman et al., 2011; Stroeven et al., 2016). Because of the  
376 short  $^{14}\text{C}$  half-life and an improved sampling methodology, *in situ*  $^{14}\text{C}$  may now be a prime candidate  
377 nuclide to be included in last deglaciation studies on glaciated cratons, such as the dating of boulders

378 deposited along glacial flowlines; a technique practiced successfully using  $^{10}\text{Be}$  (Margold et al., 2019;  
379 Norris et al., 2022).

380

## 381 **6. Conclusion**

382 Ten *in situ*  $^{14}\text{C}$  measurements on bedrock are consistent with a RSL curve for Forsmark derived from  
383 organic radiocarbon dating of basal sediments in isolation basins and the Fennoscandian Ice Sheet  
384 deglaciation chronologies from Stroeven et al. (2016) and Hughes et al. (2016). This study introduces  
385 the use of *in situ*  $^{14}\text{C}$  in Fennoscandian Ice Sheet paleoglaciology and outlines a promise of its use as a  
386 basis for supporting future shoreline displacement studies and for tracking the deglaciation in areas  
387 that lack datable organic material and where  $^{10}\text{Be}$  and  $^{26}\text{Al}$  routinely return complex exposure results.

388

389 **Data availability.** Data are available in Supplements 1-3. LiDAR data used in the study are available  
390 from <https://www.lantmateriet.se>

391 **Author contributions.** BWG and APS initiated the study, with support from KH and JON, and drafted  
392 the manuscript. BWG, APS, and AL did the sampling. AL did petrological analyses of the sampled  
393 bedrock. NAL completed sample preparation for AMS and provided the results. JH carried out  
394 cosmogenic nuclide production rate and exposure age calculations. MWC oversaw the AMS. All  
395 authors revised the manuscript.

396 **Competing interests.** The contact author has declared that none of the authors has any competing  
397 interests.

398 **Disclaimer.** Publisher's note: Copernicus Publications remains neutral with regard to jurisdictional  
399 claims in published maps and institutional affiliations.

400 **Acknowledgements.** We thank Johan Liakka (SKB) for his support in completing this study and  
401 Nicolás Young and an anonymous reviewer for comments that improved this manuscript.

402 **Financial support.** This research was supported by the Swedish Nuclear Fuel and Waste Management  
403 Company.

404 **Review statement.** This paper was edited by Pieter Vermeesch and reviewed by Nicolás Young and  
405 an anonymous reviewer.

## 406 **References**

407 Alexanderson, H., Hättestrand, M., Lindqvist, M. A., Sigfusdottir, T.: MIS 3 age of the Veiki moraine in  
408 N Sweden - Dating the landform record of an intermediate-sized ice sheet in Scandinavia, Arctic,  
409 Antarctic, and Alpine Research, 54, 239-261, 2022.

410 Balco, G., Stone, J. O., Lifton, N. A., Dunai, T. J.: A complete and easily accessible means of calculating  
411 surface exposure ages or erosion rates from  $^{10}\text{Be}$  and  $^{26}\text{Al}$  measurements, Quaternary  
412 Geochronology, 3, 174–195, 2008.



- 413 Berglund, M.: The Holocene shore displacement of Gästrikland, eastern Sweden: a contribution to  
 414 the knowledge of Scandinavian glacio-isostatic uplift, *Journal of Quaternary Science*, 20, 519–531,  
 415 2005.
- 416 Bergström, E.: Late Holocene distribution of lake sediment and peat in NE Uppland, Sweden, SKB R-  
 417 01-12, Svensk Kärnbränslehantering AB, 2001.
- 418 Bierman, P. R., Rood, D. H., Shakun, J. D., Portenga, E. W., Corbett, L. B.: Directly dating postglacial  
 419 Greenlandic land-surface emergence at high resolution using *in situ*  $^{10}\text{Be}$ , *Quaternary Research*, 90,  
 420 110-126, 2018.
- 421 Blake, Jr., W.: Holocene emergence along the Ellesmere Island coast of northernmost Baffin Bay,  
 422 *Norsk Geologisk Tidsskrift*, 73, 147–160, 1993.
- 423 Borchers, B., Marrero, S., Balco, G., Caffee, M., Goehring, B., Lifton, N., Nishiizumi, K., Phillips, F.,  
 424 Schaefer, J., Stone, J.: Geological calibration of spallation production rates in the CRONUS Earth  
 425 project, *Quaternary Geochronology*, 31, 188–198, 2016.
- 426 Bradwell, T., Fabel, D., Clark, C. D., Chiverrell, R. C., Small, D., Smedley, R. K., Saher, M. H., Moreton,  
 427 S. G., Dove, D., Callard, S. L., Duller, G. A. T., Medialdea, A., Bateman, M. D., Burke, M. J., McDonald,  
 428 N., Gilgannon, S., Morgan, S., Roberts, D. H., Ó Cofaigh, C.: Pattern, style and timing of British-Irish Ice  
 429 Sheet advance and retreat over the last 45 000 years: evidence from NW Scotland and the adjacent  
 430 continental shelf, *Journal of Quaternary Science*, 36, 871–933, 2021.
- 431 Briner, J. P., Gosse, J. C., Bierman, P. R.: Applications of cosmogenic nuclides to Laurentide Ice Sheet  
 432 history and dynamics, *Geological Society of America, Special Paper*, 415, 29-41, 2006.  
 433
- 434 Briner, J. P., Lifton, N. A., Miller, G. H., Refsnider, K., Anderson, R. K., Finkel, R.: Using *in situ*  
 435 cosmogenic  $^{10}\text{Be}$ ,  $^{14}\text{C}$ , and  $^{26}\text{Al}$  to decipher the history of polythermal ice sheets, *Quaternary*  
 436 *Geochronology*, 19, 4–13, 2014.
- 437 Brunnberg, L.: Clay-varve Chronology and Deglaciation during the Younger Dryas and Preboreal in the  
 438 Easternmost Part of the Middle Swedish Ice Marginal Zone, Department of Quaternary Research,  
 439 Quaternaria A2, Stockholm University, Stockholm, 1-94, 1995.
- 440 Dalton, A.S., Dulfer, H.E., Margold, M., Heyman, J., Clague, J.J., Froese, D.G., Gauthier, M.S., Hughes,  
 441 A.L.C., Jennings, C.E., Norris, S.L., Stoker, B.J.: Deglaciation of the north American ice sheet complex  
 442 in calendar years based on a comprehensive database of chronological data: NADI-1, *Quaternary*  
 443 *Science Reviews*, 321, 108345, 2023.
- 444 Dalton, A. S., Margold, M., Stokes, C. R., Tarasov, L., Dyke, A. S., Adams, R. S., Allard, S., Arends, H. E.,  
 445 Atkinson, N., Attig, J. W., Barnett, P. J., Barnett, R. L., Batterson, M., Bernatchez, P., Borns Jr., H. W.,  
 446 Breckenridge, A., Briner, J. P., Brouard, E., Campbell, J. E., Carlson, A. E., Clague, J. J., Curry, B. B.,  
 447 Daigneault, R. A., Dubé-Loubert, H., Easterbrook, D. J., Franzi, D. A., Friedrich, H. G., Funder, S.,  
 448 Gauthier, M. S., Gowan, A. S., Harris, K. L., Hétu, B., Hooyer, T. S., Jennings, C. E., Johnson, M. D.,  
 449 Kehew, A. E., Kelley, S. E., Kerr, D., King, E. L., Kjeldsen, K. K., Knaeble, A. R., Lajeunesse, P., Lakeman,  
 450 T. R., Lamothe, M., Larson, P., Lavoie, M., Loope, H. M., Lowell, T. V., Lusardi, B. A., Manz, L.,  
 451 McMartin, I., Nixon, F. C., Occhietti, S., Parkhill, M. A., Piper, D. J. W., Pronk, A. G., Richard, P. J. H.,  
 452 Ridge, J. C., Ross, M., Roy, M., Seaman, A., Shaw, J., Stea, R. R., Teller, J. T., Thompson, W. B.,  
 453 Thorleifson, L. H., Utting, D. J., Veillette, J. J., Ward, B. C., Weddle, T. K., Wright, H. E.: An updated  
 454 radiocarbon-based ice margin chronology for the last deglaciation of the North American Ice Sheet  
 455 Complex, *Quaternary Science Reviews*, 234, 106223, 2020.

- 456 De Geer, G.: The transbaltic extension of the Swedish Time Scale, *Geografiska Annaler*, 17, 533-549,  
457 1935.
- 458 De Geer, G.: *Geochronologia Suecica* principles, *Kungliga svenska vetenskapsakademien Handlingar*,  
459 III, Bd 18, 6, 1–367, 1940.
- 460 Dyke, A. S., Morris, T. F., Green, D. E. C., England, J.: Quaternary geology of Prince of Wales Island,  
461 Arctic Canada, *Geological Survey of Canada, Memoir*, 433, 1–142, 1992.
- 462 Dyke, A. S., Andrews, J. T., Clark, P. U., England, J. H., Miller, G. H., Shaw, J., Veillette, J. J.: The  
463 Laurentide and Innuitian ice sheets during the Last Glacial Maximum, *Quaternary Science Reviews*,  
464 21, 9–31, 2002.
- 465 Fogwill, C., Turney, C., Golledge, N., Rood, D., Hippe, K., Wacker, L., Jones, R.: Drivers of abrupt  
466 Holocene shifts in West Antarctic ice stream direction determined from combined ice sheet  
467 modelling and geologic signatures. *Antarctic Science*, 26, 674–686, 2014.
- 468 Goehring, B. M., Schaefer, J. M., Schluechter, C., Lifton, N. A., Finkel, R. C., Jull, A. J. T., Akçar, N.,  
469 Alley, R. B.: The Rhone Glacier was smaller than today for most of the Holocene, *Geology*, 39, 679–  
470 682, 2011.
- 471 Gosse, J. C., Phillips, F. M.: Terrestrial *in situ* cosmogenic nuclides: theory and application, *Quaternary*  
472 *Science Reviews*, 20, 1475–1560, 2001.
- 473 Greenwood, S. L., Simkins, L. M., Winsborrow, M. C. M., Bjarnadottir, L. R.: Exceptions to bed-  
474 controlled ice sheet flow and retreat from glaciated continental margins worldwide, *Science*  
475 *Advances*, 7, eabb6291, 2021.
- 476 Greenwood, S. L., Clason, C. C., Nyberg, J., Jakobsson, M., Holmlund, P.: The Bothnian Sea ice stream:  
477 early Holocene retreat dynamics of the south-central Fennoscandian Ice Sheet, *Boreas*, 46, 346-362,  
478 2017.
- 479 Hall A. M., Ebert K., Goodfellow B. W., Hättstrand C., Heyman J., Krabbendam M., Moon S., Stroeven  
480 A. P.: Past and future impact of glacial erosion in Forsmark and Uppland. TR-19-07 Svensk  
481 Kärnbränslehantering AB, 2019.
- 482 Hall, A. M., Krabbendam, M., van Boeckel, M., Goodfellow, B. W., Hättstrand, C., Heyman, J.,  
483 Palamakumbura, R. N., Stroeven A. P., Näslund, J.-O.: Glacial ripping: geomorphological evidence  
484 from Sweden for a new process of glacial erosion, *Geografiska Annaler*, 102, 333-353, 2020.
- 485 Hedenström, A., Risberg, J.: Shore displacement in northern Uppland during the last 6500 calendar  
486 years, TR-03-17 Svensk Kärnbränslehantering AB, 2003.
- 487 Heyman, J., Stroeven, A. P., Harbor, J. M., Caffee, M. W.: Too young or too old: Evaluating  
488 cosmogenic exposure dating based on an analysis of compiled boulder exposure ages, *Earth and*  
489 *Planetary Science Letters*, 302, 71–80, 2011.
- 490 Hippe, K., Lifton, N. A.: Calculating isotope ratios and nuclide concentrations for *in situ* cosmogenic  
491  $^{14}\text{C}$  Analyses, *Radiocarbon*, 56, 1167–1174, 2014.
- 492 Hippe, K., Ivy-Ochs, S., Kober, F., Zasadni, J., Wieler, R., Wacker, L., Kubik, P.W., Schlüchter, C.:  
493 Chronology of Lateglacial ice flow reorganization and deglaciation in the Gotthard Pass area, Central  
494 Swiss Alps, based on cosmogenic  $^{10}\text{Be}$  and *in situ*  $^{14}\text{C}$ , *Quaternary Geochronology*, 19, 14–26, 2014.

495 Hughes, A. L. C., Gyllencreutz, R., Lohne, Ø. S., Mangerud, J., Svendsen, J. I.: The last Eurasian ice  
496 sheets – a chronological database and time-slice reconstruction, *DATED-1, Boreas*, 45, 1–45, 2016.

497 Ivy-Ochs, S., Kober, F.: Surface exposure dating with cosmogenic nuclides, *Quaternary Science*  
498 *Journal*, 57, 157–189, 2008.

499 Kleman, J., Hättestrand, M., Borgström, I., Preusser, F., Fabel, D.: The Idre marginal moraine—an  
500 anchorpoint for Middle and Late Weichselian ice sheet chronology, *Quaternary Science Advances*, 2,  
501 100010, 2020.

502 Kleman, J., Stroeven, A. P., Lundqvist, J.: Patterns of Quaternary ice sheet erosion and deposition in  
503 Fennoscandia and a theoretical framework for explanation, *Geomorphology*, 97, 73–90, 2008.

504 Koester, A., Lifton, N. A.: Technical note: A software framework for calculating compositionally  
505 dependent *in situ* <sup>14</sup>C production rates, *Geochronology*, 5, 21–33, 2023.

506 Lal, D.: Cosmic ray labeling of erosion surfaces: *in situ* nuclide production rates and erosion rates,  
507 *Earth and Planetary Science Letters*, 104, 424–439, 1991.

508 Lambeck, K., Purcell, A., Zhao, J., Svensson, N.-O.: The Scandinavian Ice Sheet: from MIS 4 to the end  
509 of the Last Glacial Maximum, *Boreas*, 39, 410-435, 2010.

510 Lambeck, K., Smither, C., Johnston, P.: Sea-level change, glacial rebound and mantle viscosity for  
511 northern Europe, *Geophysical Journal International*, 134, 102-134, 1998.

512 Lidberg, M., Johansson, J. M., Scherneck, H.-G., Milne, G. A.: Recent results based on continuous GPS  
513 observations of the GIA process in Fennoscandia from BIFROST, *Journal of Geodynamics*, 50, 8–18,  
514 2010.

515 Lifton, N.: Implications of two Holocene time-dependent geomagnetic models for cosmogenic nuclide  
516 production rate scaling, *Earth and Planetary Science Letters*, 433, 257–268, 2016.

517 Lifton, N., Caffee, M., Finkel, R., Marrero, S., Nishiizumi, K., Phillips, F. M., Goehring, B., Gosse, J.,  
518 Stone, J., Schaefer, J., Theriault, B.: *In situ* cosmogenic nuclide production rate calibration for the  
519 CRONUS-Earth project from Lake Bonneville, Utah, shoreline features, *Quaternary Geochronology*,  
520 26, 56–69, 2015.

521 Lifton, N., Sato, T., and Dunai, T. J.: Scaling *in situ* cosmogenic nuclide production rates using  
522 analytical approximations to atmospheric cosmic-ray fluxes, *Earth and Planetary Science Letters*, 386,  
523 149–160, 2014.

524 Lifton, N., Wilson, J., Koester, A.: Technical note: Studying Li-metaborate fluxes and extraction  
525 protocols with a new, fully automated *in situ* cosmogenic <sup>14</sup>C processing system at PRIME Lab,  
526 *Geochronology*, 5, 361–375, 2023.

527 Long, A. J., Woodroffe, S. A., Roberts, D. H., Dawson, S.: Isolation basins, sea-level changes and the  
528 Holocene history of the Greenland Ice Sheet, *Quaternary Science Reviews*, 30, 3748–3768, 2011.

529 Lönqvist, M., Hökmark, H.: Approach to estimating the maximum depth for glacially induced  
530 hydraulic jacking in fractured crystalline rock at Forsmark, Sweden, *Journal of Geophysical Research:*  
531 *Earth Surface*, 118, 1777–1791, 2013.

532 Lupker, M., Hippe, K., Wacker, L., Kober, F., Maden, C., Braucher, R., Bourlès, D., Romani, J. R. V.,  
533 Wieler, R.: Depth-dependence of the production rate of *in situ* <sup>14</sup>C in quartz from the Leymon High  
534 core, Spain, *Quaternary Geochronology*, 28, 80–87, 2015.

535 Margold, M., Gosse, J. C., Hidy, A. J., Woywitka, R. J., Young, J. M., Froese, D.: Beryllium-10 dating of  
536 the Foothills Erratics Train in Alberta, Canada, indicates detachment of the Laurentide Ice Sheet from  
537 the Rocky Mountains at ~15 ka, *Quaternary Research*, 92, 469–482, 2019.

538 Marrero, S. M., Phillips, F. M., Caffee, M. W., Gosse, J. C.: CRONUS-Earth cosmogenic <sup>36</sup>Cl calibration,  
539 *Quaternary Geochronology*, 31, 199–219, 2016.

540 Matmon, A., Crouvi, O., Enzel, Y., Bierman, P., Larsen, J., Porat, N., Amit, R., Caffee, M.: Complex  
541 exposure histories of chert clasts in the late Pleistocene shorelines of Lake Lisan, southern Israel.  
542 *Earth Surface Processes and Landforms* 28, 493–506, 2003.

543 Miller, G. H., Briner, J. P., Lifton, N. A., Finkel, R. C.: Limited ice-sheet erosion and complex exposure  
544 histories derived from *in situ* cosmogenic <sup>10</sup>Be, <sup>26</sup>Al, <sup>14</sup>C on Baffin Island, Arctic Canada, *Quaternary*  
545 *Geochronology*, 1, 74–85, 2006.

546 Moon, S., Perron, J. T., Martel, S.J., Goodfellow, B.W., Mas Ivars, D., Hall, A., Heyman, J., Munier, R.,  
547 Näslund, J.-O., Simeonov, A., Stroeven, A.P.: Present-day stress field influences bedrock fracture  
548 openness deep into the subsurface. *Geophysical Research Letters* 47, e2020GL090581, 2020.

549 Norris, S. L., Tarasov, L., Monteath, A. J., Gosse, J. C., Hidy, A. J., Margold, M., Froese, D. G.: Rapid  
550 retreat of the southwestern Laurentide Ice Sheet during the Bølling-Allerød interval, *Geology*, 50,  
551 417–421, 2022.

552 Påsse, T., Andersson, L: Shore-level displacement in Fennoscandia calculated from empirical data,  
553 *GFF*, 127, 253–268, 2005.

554 Patton, H., Hubbard, A., Andreassen, K., Auriac, A., Whitehouse, P. L., Stroeven, A. P., Shackleton, C.,  
555 Winsborrow, M., Heyman, J., Hall, A. M.: Deglaciation of the Eurasian ice sheet complex, *Quaternary*  
556 *Science Reviews*, 169, 148–172, 2017.

557 Patton, H., Hubbard, A., Andreassen, K., Winsborrow, M., Stroeven, A.P.: The build-up, configuration,  
558 and dynamical sensitivity of the Eurasian ice-sheet complex to Late Weichselian climatic and oceanic  
559 forcing, *Quaternary Science Reviews*, 153, 97–121, 2016.

560 Patton, H., Hubbard, A., Heyman, J., Alexandropoulou, N., Lasabuda, A. P. E., Stroeven, A.P., Hall,  
561 A.M., Winsborrow, M., Sugden, D.E., Kleman, J., Andreassen, K.: The extreme yet transient nature of  
562 glacial erosion, *Nature Communications* 13, 7377, 2022.

563 Pendleton, S., Miller, G., Lifton, N., Young, N.: Cryosphere response resolves conflicting evidence for  
564 the timing of peak Holocene warmth on Baffin Island, Arctic Canada, *Quaternary Science*  
565 *Reviews*, 216, 107–115, 2019.

566 Phillips, F. M., Argento, D. C., Balco, G., Caffee, M. W., Clem, J., Dunai, T. J., Finkel, R., Goehring, B.,  
567 Gosse, J. C., Hudson, A. M., Jull, A. J. T., Kelly, M. A., Kurz, M., Lal, D., Lifton, N., Marrero, S. M.,  
568 Nishiizumi, K., Reedy, R. C., Schaefer, J., Stone, J. O. H., Swanson, T., Zreda, M. G.: The CRONUS-Earth  
569 Project: A synthesis, *Quaternary Geochronology*, 31, 119–154, 2016.

570 Rainio, H., Kejonen, A., Kielosto, S., Lahermo, P.: Avancerade inlandsisen på nytt också till  
571 Mellanfinska randformationen? *Geologi*, 38, 95–109, 1986.

572 Regnéll, C., Becher, G. P., Öhrling, C., Greenwood, S. L., Gyllencreutz, R., Blomdin, R., Brendryen, J.,  
573 Goodfellow, B. W., Mikko, H., Ransed, G., Smith, C.: Ice-dammed lakes and deglaciation history of the  
574 Scandinavian Ice Sheet in central Jämtland, Sweden, *Quaternary Science Reviews*, 314, 108219, 2023.

- 575 Risberg, J.: Strandförskjutningen i nordvästra Uppland under subboreal tid. In Segerberg, A. Bälinge  
576 mossar: kustbor i Uppland under yngre stenålder, PhD Thesis. Uppsala University, Appendix 4. (in  
577 Swedish), 1999.
- 578 Robertsson, A.-M., Persson, C.: Biostratigraphical studies of three mires in northern Uppland,  
579 Sweden, Sveriges geologiska undersökning, (Serie C 821.), 1989.
- 580 Romundset, A., Bondevik, S., Bennike, O.: Postglacial uplift and relative sea level changes in  
581 Finnmark, northern Norway, Quaternary Science Reviews, 30, 2398–2421, 2011.
- 582 Schildgen, T. F., Phillips, W. M., Purves, R. S.: Simulation of snow shielding corrections for cosmogenic  
583 nuclide surface exposure studies, Geomorphology, 64, 67–85, 2005.
- 584 Schimmelpfennig, I., Schaefer, J. M., Goehring, B. M., Lifton, N., Putnam, A. E., Barrell, D. J.:  
585 Calibration of the *in situ* cosmogenic <sup>14</sup>C production rate in New Zealand's Southern Alps, Journal of  
586 Quaternary Science, 27, 671–674, 2012.
- 587 Schimmelpfennig, I., Schaefer, J. M., Lamp, J., Godard, V., Schwartz, R., Bard, E., Tuna, T., Akçar, N.,  
588 Schlüchter, C., Zimmerman, S., and ASTER Team: Glacier response to Holocene warmth inferred from  
589 *in situ* <sup>10</sup>Be and <sup>14</sup>C bedrock analyses in Steingletscher's forefield (central Swiss Alps), Climate of the  
590 Past, 18, 23–44, 2022.
- 591 Schweinsberg, A. D., Briner, J. P., Miller, G. H., Lifton, N. A., Bennike, O., & Graham, B. L.: Holocene  
592 mountain glacier history in the Sukkertoppen Iskappe area, southwest Greenland, Quaternary  
593 Science Reviews, 197, 142–161, 2018.
- 594 SGU: Högsta Kustlinjen (in Swedish) [https://resource.sgu.se/dokument/produkter/hogsta-kustlinjen-](https://resource.sgu.se/dokument/produkter/hogsta-kustlinjen-beskrivning)  
595 [beskrivning](https://resource.sgu.se/dokument/produkter/hogsta-kustlinjen-beskrivning) (Geological Survey of Sweden), 2015.
- 596 Simkins, L. M., Simms, A. R., DeWitt, R.: Relative sea-level history of Marguerite Bay, Antarctic  
597 Peninsula derived from optically stimulated luminescence-dated beach cobbles, Quaternary Science  
598 Reviews, 77, 141–155, 2013.
- 599 SKB: Post-closure safety for the final repository for spent nuclear fuel at Forsmark – Climate and  
600 climate-related issues, PSAR version, TR-20-12, Svensk Kärnbränslehantering AB, 2020.
- 601 SKB: Post-closure safety for the final repository for spent nuclear fuel at Forsmark – Main report,  
602 PSAR version. SKB TR-21-01, Svensk Kärnbränslehantering AB, 2022.
- 603 Steffen, H., Wu, P.: Glacial isostatic adjustment in Fennoscandia - A review of data and modeling,  
604 Journal of Geodynamics, 52, 169–204, 2011.
- 605 Steinemann, O., Ivy-Ochs, S., Hippe, K., Christl, M., Haghypour, N., and Synal, H. A.: Glacial erosion by  
606 the Trift glacier (Switzerland): Deciphering the development of riegels, rock basins and gorges,  
607 Geomorphology, 375, 107533, 2021.
- 608 Stephens, M. B., Jansson, N. F.: Chapter 6, Paleoproterozoic (1.9–1.8 Ga) syn-orogenic magmatism,  
609 sedimentation and mineralization in the Bergslagen lithotectonic unit, Svecokarelian orogen. In M B  
610 Stephens & J Bergman Weihed (eds.): Sweden: Lithotectonic Framework, Tectonic Evolution and  
611 Mineral Resources, Geological Society of London Memoirs, 50, 105–206, 2020.

- 612 Stroeven, A. P., Hättestrand, C., Kleman, J., Heyman, J., Fabel, D., Fredin, O., Goodfellow, B. W.,  
613 Harbor, J. M., Jansen, J. D., Olsen, L., Caffee, M. W., Fink, D., Lundqvist, J., Rosqvist, G. C., Strömberg,  
614 B., Jansson, K. N.: Deglaciation of Fennoscandia, *Quaternary Science Reviews*, 147, 91–12, 2016.
- 615 Stroeven, A.P., Heyman, J., Fabel, D., Björck, S., Caffee, M.W., Fredin, O., Harbor, J.M.: A new  
616 Scandinavian reference  $^{10}\text{Be}$  production rate, *Quaternary Geochronology*, 29, 104–115, 2015.
- 617 Strömberg, B.: Late Weichselian deglaciation and clay varve chronology in east-central Sweden,  
618 *Sveriges geologiska undersökning (Ser. Ca 73)*, 1989.
- 619 Strömberg, B.: Younger Dryas deglaciation at Mt. Billingen, and clay varve dating of the Younger  
620 Dryas/Preboreal transition, *Boreas*, 23, 177-193, 1994.
- 621 Wohlfarth, B., Björck, S., Possnert, G.: The Swedish Time Scale: a potential calibration tool for the  
622 radiocarbon time scale during the late Weichselian, *Radiocarbon*, 37, 347-359, 1995.
- 623 Young, N. E., Lesnek, A. J., Cuzzone, J. K., Briner, J. P., Badgeley, J. A., Balter-Kennedy, A., Graham, B.  
624 L., Cluett, A., Lamp, J. L., Schwartz, R., Tuna, T., Bard, E., Caffee, M. W., Zimmerman, S. R. H.,  
625 Schaefer, J. M.: *In situ* cosmogenic  $^{10}\text{Be}$ – $^{14}\text{C}$ – $^{26}\text{Al}$  measurements from recently deglaciated bedrock as  
626 a new tool to decipher changes in Greenland Ice Sheet size, *Climate of the Past*, 17, 419–450, 2021.
- 627 Young, N. E., Schaefer, J. M., Goehring, B., Lifton, N., Schimmelpfennig, I., Briner, J. P.: West  
628 Greenland and global *in situ*  $^{14}\text{C}$  production-rate calibrations, *Journal of Quaternary Science*, 29, 401–  
629 406, 2014.